Kinetics, Mechanism, and Thermochemistry of the Gas Phase Reaction of Atomic Chlorine with Dimethyl Sulfoxide†

J. M. Nicovich,‡ S. Parthasarathy,§ F. D. Pope,‡,# A. T. Pegus,‡,|| M. L. McKee,⊥ and P. H. Wine*,‡,§

School of Chemistry & Biochemistry, Georgia Institute of Technology, Atlanta, Georgia 30332-0400, School of Earth & Atmospheric Sciences, Georgia Institute of Technology, Atlanta, Georgia 30332-0340, and Department of Chemistry & Biochemistry, Auburn University, Auburn, Alabama 36849

Received: November 21, 2005; In Final Form: January 18, 2006

A laser flash photolysis−resonance fluorescence technique has been employed to study the kinetics of the reaction of chlorine atoms with dimethyl sulfoxide ($CH_3S(O)CH_3$; DMSO) as a function of temperature (270−571 K) and pressure (5−500 Torr) in nitrogen bath gas. At $T = 296$ K and $P \geq 5$ Torr, measured rate coefficients increase with increasing pressure. Combining our data with literature values for low-pressure rate coefficients (0.5−3 Torr He) leads to a rate coefficient for the pressure independent H-transfer channel of $k_{1a} = 1.45 \times 10^{-11}$ cm^3 molecule^{-1} s^{-1} and the following falloff parameters for the pressure-dependent addition channel in N_2 bath gas: $k_{1b,0} = 2.53 \times 10^{-28}$ cm^6 molecule^{-2} s^{-1}; $k_{1b,\infty} = 1.17 \times 10^{-10}$ cm^3 molecule^{-1} s^{-1}, $F_c = 0.503$. At the 95% confidence level, both k_{1a} and $k_{1b}(P)$ have estimated accuracies of ±30%. At $T > 430$ K, where adduct decomposition is fast enough that only the H-transfer pathway is important, measured rate coefficients are independent of pressure (30−100 Torr N_2) and increase with increasing temperature. The following Arrhenius expression adequately describes the temperature dependence of the rate coefficients measured at over the range 438−571 K: $k_{1a} = (4.6 \pm 0.4) \times 10^{-11} \exp[-(472 \pm 40)/T)$ cm^3 molecule^{-1} s^{-1} (uncertainties are 2σ, precision only). When our data at $T > 430$ K are combined with values for k_{1a} at temperatures of 273−335 K that are obtained by correcting reported low-pressure rate coefficients from discharge flow studies to remove the contribution from the pressure-dependent channel, the following modified Arrhenius expression best describes the derived temperature dependence: $k_{1a} = 1.34 \times 10^{-15} T^{1.40} \exp(+383/T)$ cm^3 molecule^{-1} s^{-1} (273 K ≤ T ≤ 571 K). At temperatures around 330 K, reversible addition is observed, thus allowing equilibrium constants for Cl−DMSO formation and dissociation to be determined. A third-law analysis of the equilibrium data using structural information obtained from electronic structure calculations leads to the following thermochemical parameters for the association reaction: $\Delta_r H°_{298} = -72.8 \pm 2.9$ kJ mol^{-1}, $\Delta H°_0 = -71.5 \pm 3.3$ kJ mol^{-1}, and $\Delta_r S°_{298} = -110.6 \pm 4.0$ J K^{-1} mol^{-1}. In conjunction with standard enthalpies of formation of Cl and DMSO taken from the literature, the above values for $\Delta_r H°$ lead to the following values for the standard enthalpy of formation of Cl−DMSO: $\Delta_f H°_{298} = -102.7 \pm 4.9$ kJ mol^{-1} and $\Delta_r H°_0 = -84.4 \pm 5.8$ kJ mol^{-1}. Uncertainties in the above thermochemical parameters represent estimated accuracy at the 95% confidence level. In agreement with one published theoretical study, electronic structure calculations using density functional theory and G3B3 theory reproduce the experimental adduct bond strength quite well.

Introduction

Dimethyl sulfoxide ($CH_3S(O)CH_3$; DMSO) is an important intermediate in the atmospheric oxidation of dimethyl sulfide (CH_3SCH_3; DMS).[1−7] DMS is produced primarily via biological activity in seawater, and its release from the oceans to the atmosphere is thought to be the largest natural source of atmospheric sulfur.[8−11] The atmospheric oxidation of DMS may play an important role in global climate because nonvolatile DMS oxidation products can contribute to aerosol formation and growth in the remote marine environment,[12−14] thus impacting climate directly via aerosol scattering of solar radiation and indirectly via modification of cloud properties.[12,15,16] The current incomplete knowledge of the DMS oxidation mechanism inhibits an accurate assessment of its role as a source of nonvolatile gases such as sulfuric acid (H_2SO_4) and methane sulfonic acid ($CH_3(O)S(O)OH$; MSA);[17,18] these gases are thought to play important roles in particle formation and growth.[10]

Atmospheric DMSO is known to be formed in substantial yield from the reaction of the weakly bound OH−DMS adduct with O_2,[6,7,19,20] and in essentially unit yield from the reaction of BrO radicals with DMS.[21−23] The OH + DMSO reaction is quite fast[5,24−28] and appears to be the dominant gas-phase atmospheric removal mechanism for DMSO, although uptake into the atmospheric condensed phase and subsequent condensed

† Part of the special issue "David M. Golden Festschrift".

* To whom correspondence should be addressed.
‡ School of Chemistry & Biochemistry, Georgia Institute of Technology.
§ School of Earth & Atmospheric Sciences, Georgia Institute of Technology.
# Now at Jet Propulsion Laboratory, M/S 183-901, 4800 Oak Grove Dr., Pasadena, CA 91109.
|| Now at Department of Chemistry, Imperial College, Exhibition Rd., London SW7 2AZ, U.K.
⊥ Auburn University.

10.1021/jp0567467 CCC: $33.50
Published on Web 03/15/2006

phase reaction also appears to be an important loss mechanism.[1,27,29,30−33] The reaction of atomic chlorine with DMSO,

$$Cl + CH_3S(O)CH_3 \rightarrow \text{products} \quad (1)$$

is at most a minor sink for atmospheric DMSO. However, characterization of the overall reaction kinetics as a function of temperature and pressure, the branching ratios for H-transfer and adduct formation, and the bond strength of the Cl−DMSO adduct are of interest for establishing reactivity trends in radical + organosulfur compound reactions (many of which are atmospherically important), and for testing the ability of electronic structure theory and reaction rate theory to predict or rationalize the observed trends.

Four experimental studies of Cl + DMSO reaction kinetics are reported in the literature.[24,27,34,35] Barnes et al.[24] carried out a relative rate study at room temperature and atmospheric pressure (using propene as the competitor) and obtained rate coefficients of 7.4×10^{-11} cm^3 molecule^{-1} s^{-1} in air and 5.4×10^{-11} cm^3 molecule^{-1} s^{-1} in nitrogen. Falbe-Hansen et al.[27] also carried out a relative rate study at room temperature and atmospheric pressure (using ethane and propane as competitors) and obtained a rate coefficient of 7.4×10^{-11} cm^3 molecule^{-1} s^{-1} in air, in excellent agreement with the findings of Barnes et al.[24] The first absolute kinetics study of reaction 1 was reported by Martinez et al.,[34] who employed a low-pressure discharge flow technique with mass spectrometric detection to investigate Cl + DMSO kinetics in helium bath gas over the pressure range 0.5−3 Torr and the temperature range 273−335 K. Martinez et al. report rate coefficients in the range $(1.4-2.0) \times 10^{-11}$ cm^3 molecule^{-1} s^{-1} with no discernible temperature or pressure dependence and also report that HCl is not observed as a reaction product, although their detection sensitivity for HCl appeared to be marginal. A second low-pressure discharge flow study of Cl + DMSO kinetics has been reported by Riffault et al.;[35] they report a rate coefficient of 2.05×10^{-11} cm^3 molecule^{-1} s^{-1} in 1 Torr of helium bath gas at $T = 298$ K, and also report that the HCl yield is 0.91 ± 0.15. The significantly lower rate coefficients reported by Martinez et al.[34] and Riffault et al.[35] compared to the values reported by Barnes et al.[24] and Falbe-Hansen et al.,[27] suggest that k_1 is pressure dependent, which, in turn, suggests that an important reaction channel is formation of a relatively stable adduct. A recent theoretical study by Vandresen and Resende predicts that Cl does indeed add to the sulfur atom in DMSO to form an adduct that is bound by 73 kJ mol^{-1} at 298 K.[36]

In this paper we report a study of Cl + DMSO kinetics that spans a much wider range of temperature and pressure than was covered in previous studies. Pressure-independent kinetics are observed at high temperature and pressure-dependent kinetics are observed at low temperature. In an intermediate temperature regime, both adduct formation and adduct decomposition are observable on the experimental time scales accessible in our laser flash photolysis experiments ($10^{-5}-10^{-2}$ s). The experimental results allow rate coefficients to be evaluated for the pressure independent pathway (presumably hydrogen transfer), the adduct formation pathway, and the adduct dissociation pathway, and also allow the adduct bond strength to be evaluated. Electronic structure calculations are also reported that provide structural information about Cl−DMSO (used in the "third law" evaluation of the bond strength) as well as an adduct bond strength that can be compared with the experimental value and with the recently published[36] theoretical value. Finally, literature values for adduct bond strengths and rate coefficients for Cl, Br, and OH reactions with DMS and DMSO are tabulated and trends are discussed.

Experimental Technique

Chlorine atom kinetics in the presence of varying amounts of DMSO, and at varying temperatures and pressures of N_2 bath gas, were studied using the laser flash photolysis (LFP)−resonance fluorescence (RF) technique. The LFP−RF apparatus was similar to those we have employed in several previous studies of chlorine atom kinetics.[37−42] A schematic diagram of the apparatus is published elsewhere.[43] Important features of the apparatus as well as experimental details that are specific to this study are summarized below.

Two different reaction cells were employed in this study. All experiments at $T \leq 330$ K employed a jacketed Pyrex reaction cell[43] with an internal volume of ∼160 cm^3. The cell was maintained at a constant temperature by circulating ethylene glycol (for $T \geq 295$ K) or a 2:1 ethanol-methanol mixture (for $T < 295$ K) from a thermostated bath through the outer jacket. All experiments at $T > 350$ K employed a quartz reaction cell with an internal volume of ∼250 cm^3. The cell was maintained at a constant temperature by passing a well-controlled current through high-resistance-wire heaters that were wrapped around it. Copper−constantan (for low-temperature studies) or chromel−alumel (for high-temperature studies) thermocouples could be injected into the reaction zone through a vacuum seal, thus allowing measurement of the gas temperature in the reaction volume (i.e., the volume from which fluorescence could be detected) under the precise pressure and flow rate conditions of the experiment. Temperature variation within the reaction volume was found to be <0.5 K at $T = 270$ K and <1.5 K at $T = 570$ K.

Chlorine atoms were produced by 248 or 266 nm laser flash photolysis of phosgene:

$$Cl_2CO + h\nu\ (248 \text{ or } 266 \text{ nm}) \rightarrow 2Cl + CO \quad (2)$$

A Lambda Physik Compex 102 KrF excimer laser served as the 248 nm light source; the pulse width was ∼20 ns and fluences employed in this study ranged from 12 to 35 mJ cm^{-2} pulse^{-1}. Fourth harmonic radiation from a Quanta Ray model DCR-2A Nd:YAG laser served as the 266 nm light source; the pulse width was ∼6 ns and fluences employed in this study ranged from 12 to 44 mJ cm^{-2} pulse^{-1}.

An atomic resonance lamp situated perpendicular to the photolysis laser excited resonance fluorescence in the photolytically generated chlorine atoms. The resonance lamp consisted of an electrodeless microwave discharge through about 1 Torr of a flowing mixture containing a trace of Cl_2 in helium. The flows of a 0.1% Cl_2 in He mixture and pure He into the lamp were controlled by separate needle valves, thus allowing the total pressure and Cl_2 concentration to be independently adjusted for optimum signal-to-noise. Radiation was coupled out of the lamp through a magnesium fluoride window and into the reaction cell through a magnesium fluoride lens. Before entering the reaction cell, the lamp output passed through a flowing gas filter containing 3 Torr-cm N_2O in N_2; this filter blocked virtually all O atom impurity emissions at 130−131 nm while transmitting the Cl atom emissions in the 135−140 nm wavelength range. Fluorescence intensities were found to vary linearly with atom concentration up to levels several times higher than any used in the kinetics experiments ($[Cl]_0 < 2 \times 10^{12}$ atoms cm^{-3} in all experiments and $<1 \times 10^{12}$ atoms cm^{-3} in nearly all experiments). Collisional quenching of the excited

states from which resonance fluorescence emanates results in approximately a factor of 3 reduction in detection sensitivity at $P = 500$ Torr N_2 compared to the sensitivity at pressures less than 10 Torr N_2. Fluorescence was collected by a magnesium fluoride lens on an axis orthogonal to both the photolysis beam and the resonance lamp beam and imaged onto the photocathode of a solar blind photomultiplier. The region between the reaction cell and the photomultiplier was purged with N_2; in addition, a calcium fluoride window was inserted into this region to prevent detection of lamp emissions at wavelengths shorter than 125 nm (Lyman-α H atom emission, for example). Signals were processed using photon counting techniques in conjunction with multichannel scaling. For each chlorine atom decay measured, signals from a large number of laser shots were averaged to obtain a well-defined temporal profile over (typically) a factor of 30 variation in the Cl atom concentration. The multichannel scalar sweep was triggered prior to the photolysis laser to allow a pre-trigger baseline to be obtained.

To avoid accumulation of photochemically generated reactive species, all experiments were carried out under "slow flow" conditions. The linear flow rate through the reactor was in the range 0.6−3.1 cm s^{-1} and the laser repetition rate was varied over the range 2−10 Hz (it was 5 Hz in most experiments). Because the direction of flow was perpendicular to the photolysis laser beam, no volume element of the reaction mixture was subjected to more than a few laser shots. Phosgene and CF_2Cl_2 were flowed into the reaction cell from 12 L Pyrex bulbs containing dilute mixtures in N_2, whereas N_2 was flowed directly from its high-pressure storage tank. DMSO was introduced into the gas mixture by bubbling N_2 through the liquid DMSO sample, then mixing this flow with the other gas flows. The partial pressures of each component other than DMSO in the reaction mixture were evaluated from mass flow rate and total pressure measurements. The methodology for evaluating the DMSO concentration in the reactor is discussed below.

Because the vapor pressure of DMSO is quite low (~0.6 Torr at 298 K[44]), it was necessary to measure the concentration of this species by UV photometry in situ in the slow flow system both upstream and downstream from the reaction cell. The light sources for the photometric measurements were zinc penray lamps, and band-pass filters were employed to isolate the 213.9 nm line. The upstream and downstream absorption cells were 100 and 150 cm in length, respectively. The upstream cell was cross-shaped with a short (7.5 cm) axis that was used to check for absorption by DMSO adsorbed to the quartz windows of the photometry cells. The absorption cross section for DMSO(g) at 213.9 nm was taken to be 5.3×10^{-18} cm^2 $molecule^{-1}$;[23,25] the uncertainty in this absorption cross section is estimated to be ±20%, which represents the largest single source of uncertainty in the reported rate coefficients. In a majority of photometric measurements, a small fraction of the measured absorbance was attributable to window-adsorbed DMSO; this fraction was typically only a few percent, although it did exceed 10% in some experiments where DMSO concentrations were low. Rejection of data points in the relatively small number of cases where window absorbance exceeded 10% of the total absorbance had a negligible effect (less than 1%) on measured rate coefficients. Differences on the order of 10% between DMSO concentrations measured in the upstream and downstream cells were not uncommon, particularly in the low temperature experiments and, in fact, the upstream cell concentration was not consistently the higher one. As for the case of the window absorbance (see above), the largest concentration gradients were observed at low DMSO concentrations, and excluding those data points from the analysis resulted in negligible changes in measured rate coefficients. For all reported kinetic data, the DMSO(g) concentration in the reaction cell is taken to be the average of the concentrations measured in the upstream and downstream absorption cells.

The Cl photolytic precursor Cl_2CO absorbs at 213.9 nm, although its absorption cross section is a factor of 42 smaller than the DMSO absorption cross section.[45] In all experiments, the flow of the Cl_2CO/N_2 mixture was added to the sum of all other flows at a point between the upstream absorption cell and the reactor; this necessitated a small dilution correction (<2%) to the concentration of DMSO measured in the upstream absorption cell. Typically, Cl_2CO was present in reaction mixtures at a level where it made a small but significant contribution to the 213.9 nm absorbance in the downstream absorption cell. To account for this interference, I_0 for the DMSO absorbance measurement was always obtained with all gases except DMSO (including Cl_2CO) flowing, and the total flow rate adjusted (by adding N_2) to be the same without DMSO flowing as it was when DMSO was present in the flowing gas mixture.

The pure gases used in this study had the following stated minimum purities: N_2, 99.999%; CF_2Cl_2, 99.9%; Cl_2CO, 99.0%; for CF_2Cl_2 and Cl_2CO, the stated purities refer to the liquid phase in the high-pressure storage cylinders. Nitrogen was used as supplied and Cl_2CO and CF_2Cl_2 were degassed at 77 K before use. The DMSO had a stated minimum purity of 99.9%. It was transferred into a bubbler fitted with high-vacuum all-Teflon stopcocks, and was introduced into the reaction cell as described above. Before initiating kinetics experiments, N_2 was bubbled through the DMSO sample for several days to remove volatile impurities.

Results and Discussion

Photodissociation of Cl_2CO at $\lambda \approx 235$ nm has been shown to be a concerted process; i.e., both chlorine atoms are produced on a time scale that is short compared to a rotational period.[46] The fraction of chlorine atoms generated in the spin−orbit excited state, $Cl(^2P_{1/2})$, is thought to be significant.[46,47] Rate coefficients for deactivation of $Cl(^2P_{1/2})$ in units of cm^3 $molecule^{-1}$ s^{-1} are 5.0×10^{-15} for N_2[43] and 3.0×10^{-10} for Cl_2CO;[47] these rate coefficients suggest that relaxation of $Cl(^2P_{1/2})$ into equilibrium with $Cl(^2P_{3/2})$ is fast compared to the rate of $Cl(^2P_{1/2})$ reaction with DMSO under the experimental conditions employed, so it can be safely assumed that all Cl + DMSO kinetic data reported in this study are representative of an equilibrium mixture of $Cl(^2P_{1/2})$ and ground-state $Cl(^2P_{3/2})$ atoms. As a check on the assumption of spin state equilibration, a number of experiments were run with CF_2Cl_2, a very efficient $Cl(^2P_{1/2})$ quencher,[48−50] added to the reaction mixture. As expected, this variation in experimental conditions had no effect on observed kinetics.

All experiments were carried out under pseudo-first-order conditions with DMSO in large excess over Cl atoms. Hence, in the absence of side reactions that remove or produce Cl atoms, the Cl atom temporal profile following the laser flash would be described by the relationship

$$\ln\{[Cl]_0/[Cl]_t\} = (k_1[DMSO] + k_3)t = k't \qquad (I)$$

where k_3 is the rate coefficient for the reaction

Cl → first-order loss by diffusion from the detector field of view and/or reaction with background impurities. (3)

TABLE 1: Summary of Kinetic Data for the Cl + DMSO Reaction at $T < 300$ K and $T > 430$ K[a,b]

T	P	no. of expts[c]	concentrations			k'_{max}	$k_1 \pm 2\sigma$ [d]
			Cl_2CO	$Cl_{t=0}$	$DMSO_{max}$		
270	5.4	8	2700−5200	5−10	8100	34600	4.20 ± 0.13
270	250	5	1700−4600	3−8	1720	21200	12.1 ± 0.4
296	4.8	5	3700	10	10500	34200	3.24 ± 0.04
296	20	6	2000	6	5380	26000	4.86 ± 0.30
296	50	6	6100	17	4320	27900	6.34 ± 0.37
296	100	7	5800	9	2730	22200	7.85 ± 0.42
296	102	12	3100	3−9	1940	19000	9.42 ± 0.78
296	250	6	3500	10	2500	25200	10.0 ± 0.4
296	402	6	4800	11	1980	20200	10.4 ± 0.5
296	505	9	2400−4700	6−12	1950	21200	10.5 ± 2.0
438[e]	101	5	1180	7	9190	14600	1.56 ± 0.06[e]
467[e]	30	5	6060	5	10000	16900	1.68 ± 0.07[e]
475	100	7	1180	5	10500	17900	1.71 ± 0.07
476	30	6	1210	6	16600	27700	1.68 ± 0.09
522	31	6	1190	5	13800	25300	1.83 ± 0.04
543[e]	30	5	4080	3	8820	17200	1.93 ± 0.01[e]
571	31	6	1570	5	13800	26900	2.01 ± 0.08

[a] Units: T (K); P (Torr); concentrations (10^{11} cm^{-3}); k'_{max} (s^{-1}); k_1 (10^{-11} cm^3 molecule^{-1} s^{-1}). [b] The photolysis wavelength was 266 nm in all experiments at 270, 296, 467, and 543 K, and 248 nm in all experiments at other temperatures. [c] Expt ≡ measurement of a single pseudo-first-order Cl decay rate. [d] Uncertainties represent precision only. [e] ~4×10^{14} CF_2Cl_2 per cm^3 added to promote more rapid equilibration of the $Cl(^2P_{3/2,1/2})$ spin−orbit states.

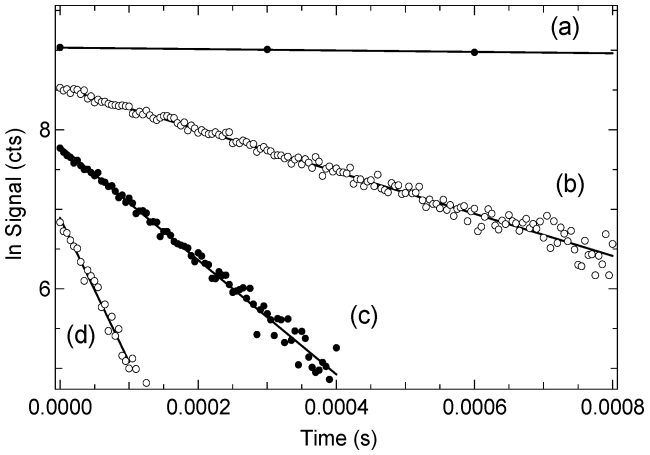

Figure 1. Typical Cl atom temporal profiles observed at $T < 300$ K and at $T > 430$ K. Experimental conditions: $T = 296$ K; $P = 102$ Torr; $[Cl_2CO] = 3.1 \times 10^{14}$ molecules cm^{-3}; $[Cl]_{t=0} = 9 \times 10^{11}$ atoms cm^{-3}; [DMSO] in units of 10^{13} molecules cm^{-3} = (a) 0, (b) 2.21, (c) 7.54, (d) 19.4. Lines are obtained from least-squares analyses and give the following pseudo-first-order decay rates in units of s^{-1}: (a) 67, (b) 2650, (c) 6950, (d) 19000.

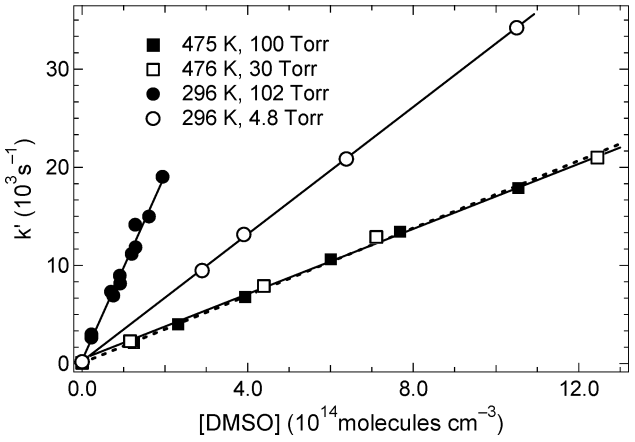

Figure 2. Plots of k', the pseudo-first-order Cl atom decay rate, versus DMSO concentration. The solid lines and the dashed line are obtained from linear least squares analyses, and the resulting bimolecular rate coefficients, i.e., the slopes of the plots, are listed in Table 1. The dashed line is the best linear fit to the data at $T = 475$ K, $P = 100$ Torr.

The bimolecular rate coefficients of interest, $k_1(P,T)$, are determined from the slopes of k' vs [DMSO] plots for data obtained at constant T and P. Observation of Cl temporal profiles that are exponential, i.e., obey eq I, a linear dependence of k' on [DMSO], and invariance of k' to variation in laser photon fluence and photolyte (i.e., phosgene) concentration strongly suggest that reactions 1 and 3 are, indeed, the only processes that significantly influence the Cl time history.

Kinetics at $T \leq 296$ K and $T \geq 438$ K. For all experiments carried out at temperatures below 300 K or above 430 K, well-behaved pseudo-first-order kinetics were observed; i.e., Cl atom temporal profiles obeyed eq I and measured k' values increased linearly with increasing [DMSO] but were independent of laser photon fluence and photolyte concentration. Typical data are shown in Figures 1 and 2, and measured bimolecular rate coefficients, $k_1(P,T)$, are summarized in Table 1. Because the precision of most of the rate coefficients reported in Table 1 is quite good, accuracy is limited primarily by the uncertainty in the DMSO concentration measurement (~20%). Hence, we estimate that the accuracy of reported values for $k_1(P,T)$ is ±25%.

At $T < 300$ K, measured bimolecular rate coefficients were found to increase with increasing pressure (see Table 1). Comparison of the pressure-dependent rate coefficients measured at 270 and 296 K in this study with the low-pressure rate coefficients at 273[34] and 298 K[34,35] reported by Martinez et al.[34] and Riffault et al.[35] demonstrates that the pressure-dependent reaction becomes the major pathway at N_2 pressures greater than a few Torr. The 296 K rate coefficients reported in this study are plotted as a function of pressure in Figure 3 along with the low-pressure 298 K rate coefficients reported by Martinez et al.[34] and Riffault et al.[35] To construct Figure 3, the pressures employed in the Martinez et al. and Riffault et al. studies are divided by two to account for the expected difference in effectiveness as a third body between N_2, which was used as the bath gas in our study, and helium, which was used as the bath gas in the studies of Martinez et al. and Riffault et al. The observed pressure dependence of k_1 suggests that the dominant reaction pathway at $T < 300$ K and pressures greater than a

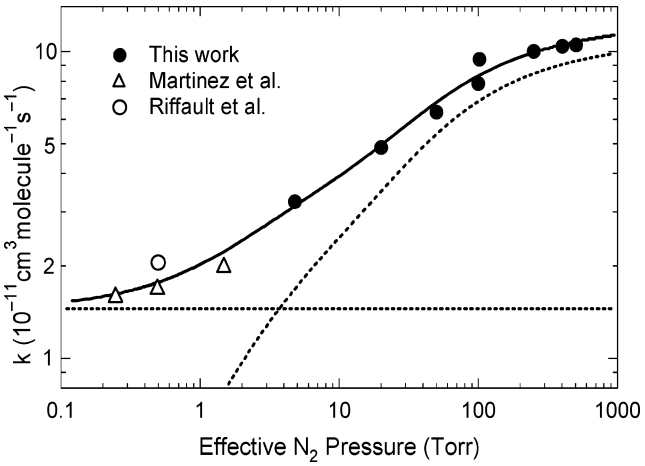

Figure 3. Plot of k_1 versus pressure for data obtained at 296−298 K. Our results over the pressure range 4.8−505 Torr are plotted along with the low-pressure results of Martinez et al.[34] and Riffault et al..[35] The solid line is the best fit to eq IV in the text; best fit parameters k_{1a}, $k_{1b,0}$, $k_{1b,\infty}$, and F_c are given in the text. The dashed lines are plots of k_{1a} versus P (horizontal line) and k_{1b} versus P.

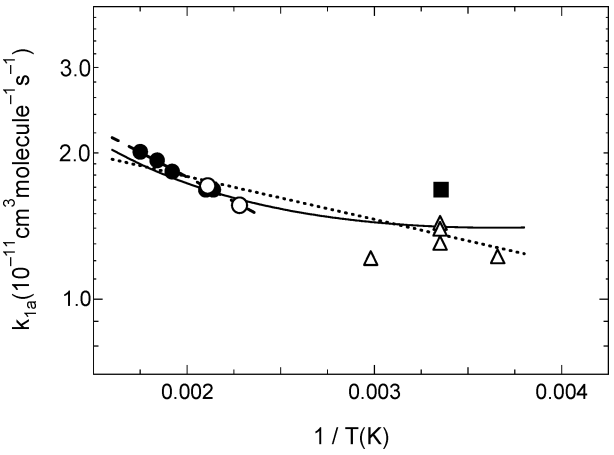

Figure 4. Arrhenius plot for the reaction Cl + $CH_3S(O)CH_3$ → $CH_3S(O)CH_2$ + HCl. Open circles: P = 100 Torr, this work; filled circles: P = 30 Torr, this work; open triangles: "corrected" data of Martinez et al.;[34] filled square: "corrected" data of Riffault et al.[35] The dashed line is the best fit of our data only to $k = A\exp(-E_a/RT)$ whereas the dotted line is the best fit of all data to the same expression. The solid line is the best fit of all data to $k = A'T^n\exp(-E_a'/RT)$. The best fit parameters that describe each of the three lines are given in the text.

few Torr is formation of a stable adduct of Cl to the sulfur atom in DMSO:

$$Cl + CH_3S(O)CH_3 + M \rightarrow CH_3(Cl)S(O)CH_3 + M \quad (1b)$$

To describe the pressure dependence of the bimolecular rate coefficient for an association reaction for a specified bath gas at a specified temperature, an equation of the following form is frequently employed:[45]

$$k([M],T) = k_0k_\infty[M]F_c^{\,X}(k_\infty + k_0[M])^{-1} \quad (II)$$

$$X = \{1 + [\log(k_0[M]/k_\infty)]^2\}^{-1} \quad (III)$$

In the above equations, k_0 and k_∞ are approximations to the low- and high-pressure limit rate coefficients, respectively, and F_c is the "broadening parameter"; k_0 and F_c depend on both temperature and the identity of the bath gas, whereas k_∞ depends only on temperature. Using the above parametrization with an added pressure-independent channel (k_{1a}), i.e.,

$$k_1 = k_{1a} + k_{1b} = k_{1a} + k_{1b,0}\,k_{1b,\infty}[M]F_c^{\,X}(k_{1b,\infty} + k_{1b,0}[M])^{-1} \quad (IV)$$

to fit the kinetic data for reaction 1 at $T = 296 \pm 2$ K gives the following results:

$$k_{1b,0}(N_2,296\text{ K}) = 2.53 \times 10^{-28}\text{ cm}^6\text{ molecule}^{-2}\text{ s}^{-1}$$

$$k_{1b,\infty}(296\text{ K}) = 1.17 \times 10^{-10}\text{ cm}^3\text{ molecule}^{-1}\text{ s}^{-1}$$

$$F_c(N_2,296\text{ K}) = 0.503$$

$$k_{1a}(296\text{ K}) = 1.45 \times 10^{-11}\text{ cm}^3\text{ molecule}^{-1}\text{ s}^{-1}$$

To obtain the above results, the four quantities $k_{1b,0}$, $k_{1b,\infty}$, F_c, and k_{1a} were all treated as adjustable parameters. As shown by the solid line in Figure 3, which is a plot of k_1 vs P, the parametrization represents the experimental data quite well. The dashed lines in Figure 3 are plots of k_{1a} vs P (horizontal line), and k_{1b} vs P. The results summarized in Figure 3 suggest that at an effective N_2 pressure of 0.5 Torr (or a helium pressure of 1.0 Torr), the pressure-independent pathway accounts for 82% of the overall reactivity, i.e., $k_{1a}/k_1 = 0.82$. Riffault et al.[35] measured the HCl yield from reaction 1 to be 0.91 ± 0.15 in 1.0 Torr of helium at 298 K. Hence, the combination of the results reported in this study and the HCl yield measurement of Riffault et al. suggests that the pressure-independent contribution to Cl + DMSO reactivity is almost exclusively hydrogen transfer:

$$Cl + CH_3S(O)CH_3 \rightarrow HCl + CH_3S(O)CH_2 \quad (1a)$$

Considering the uncertainty in determination of the DMSO concentration (see above) and the multiparameter nature of the fitting procedure used to obtain the reported value for k_{1a}, we estimate the accuracy of our k_{1a} determination to be ±30% at the 95% confidence level. As an example of the sensitivity of k_{1a} to the choice of other fit parameters, if we fix F_c at 0.6, as is done in the NASA panel evaluations,[45] the retrieved value for k_{1a} increases to 1.52×10^{-11} cm^3 molecule^{-1} s^{-1}; similarly, if we fix F_c at 0.4, the retrieved value for k_{1a} is reduced to 1.37×10^{-11} cm^3 molecule^{-1} s^{-1}. Over the range of pressure of our study (5−500 Torr), we believe that values for $k_{1b}(P)$ obtained from the reported falloff parameters are also accurate to ±30% (95% confidence level).

At $T \geq 438$ K, k_1 is found to be independent of pressure over the range 30−100 Torr (see Figure 2 and Table 1). An Arrhenius plot for reaction 1 that includes our high-temperature data is shown in Figure 4. A linear least-squares analysis of our ln k_1 vs $1/T$ data at $T > 438$ K (dashed line in Figure 4) gives the following Arrhenius expression:

$$k_1(T) = (4.6 \pm 0.4) \times 10^{-11}\exp[-(472 \pm 40)/T]\text{ cm}^3\text{ molecule}^{-1}\text{ s}^{-1} \quad (438\text{ K} \leq T \leq 571\text{ K}) \quad (V)$$

Uncertainties in the above expression are 2σ and represent the precision of the Arrhenius parameters only.

When the high-temperature kinetic observations are considered in conjunction with the kinetic and mechanistic data

TABLE 2: Results of the Cl + $CH_3S(O)CH_3$ + N_2 → $CH_3(Cl)S(O)CH_3$ + N_2 Equilibration Kinetics Experiments at T = 330 K and P = 280 Torr[a,b]

[DMSO]	Q	a	b	k_3	k_4	k_{1b}	k_{-1b}	K_p
6.31	3000	8020	530	52	238	7.28	2760	6.01
6.43[c]	3040	8150	605	45	358	7.36	2690	6.23[c]
10.6	3060	11300	592	52	192	6.88	2870	5.46
12.4	3370	14200	691	33	316	7.80	3050	5.81
12.9	3140	14200	648	33	272	7.60	2870	6.01
16.4	3220	17500	652	33	230	7.62	2990	5.79
20.7	3100	20500	675	33	237	7.29	2860	5.80
29.0	3220	25600	735	52	198	6.49	3030	4.89
33.6[c]	3130	29700	660	46	120	6.65	3010	5.04[c]
35.2	3240	31000	744	45	204	6.64	3040	4.99

[a] Units: [DMSO] (10^{13} molecules cm^{-3}); Q, a, b, k_3, k_4, k_{-1b} (s^{-1}); k_{1b} (10^{-11} cm^3 $molecule^{-1}$ s^{-1}); K_p (10^5 atm^{-1}). [b] In all experiments, $[Cl]_{t=0}$ was in the range (6−9) × 10^{11} atoms cm^{-3}, $[Cl_2CO]$ was in the range (3.5−5.1) × 10^{14} molecules cm^{-3}, and the photolysis wavelength was 248 nm. [c] ∼3 × 10^{14} CF_2Cl_2 per cm^3 added to promote more rapid equilibration of the Cl($^2P_{3/2,1/2}$) spin−orbit states.

obtained at low temperature in our laboratory and in other laboratories (discussed above and below), we are led to the conclusion that the addition pathway is unimportant at T > 430 K due to very rapid dissociation of the adduct. Hence, the dominant reaction pathway at T > 430 K is concluded to be hydrogen transfer, i.e., $k_1 = k_{1a}$. As discussed above for the room-temperature case, two recent low-pressure discharge flow (DF) kinetics studies with mass spectrometric (MS) detection of reactants and products,[34,35] when considered in conjunction with the temperature- and pressure-dependent kinetic data reported in this study, allow values for k_{1a} to be estimated at temperatures in the 273−335 K range. Plotted in Figure 4 along with the high-temperature rate coefficients measured in this study are low-pressure rate coefficients reported by Martinez et al.[34] and Riffault et al.[35] at temperatures in the range 273−335 K *with the estimated contribution from the addition channel removed*. Values of k_{1a}/k_1 at room temperature and effective N_2 pressures of 0.25, 0.5, and 1.5 Torr are taken to be 0.895, 0.82, and 0.65, respectively, on the basis of the results shown in Figure 3. To estimate k_{1a}/k_1 under the conditions of the Martinez et al. experiments at 273 and 335 K (P_{He} = 1 Torr, i.e., effective N_2 pressure of 0.5 Torr), we assume that k_{1a} is independent of temperature over the range 273−335 K, and use the values for k_{1b} that we report at 270, 296, and 330 K (see Tables 1 and 2) to estimate values of k_{1b} under the conditions of the Martinez et al. experiments. This approach leads to k_{1a}/k_1 values of 0.87 at 335 K, P_{He} = 1 Torr and 0.765 at 273 K, P_{He} = 1 Torr. When our high-temperature data are combined with the corrected low temperature, low-pressure rate coefficients, a somewhat nonlinear $ln k_{1a}$ versus T^{-1} plot is suggested. The solid line in Figure 3 is the best fit of the combined high-temperature data from this study and the low-pressure data from the DF−MS studies[34,35] (corrected using estimated values for k_{1a}/k_1 as described above) to the modified Arrhenius form $k = A'T^n \exp(-E_a'/RT)$; the best fit expression is

$$k_{1a}(T) = 1.34 \times 10^{-15} T^{1.40} \exp(+383/T)\ \mathrm{cm^3\ molecule^{-1}\ s^{-1}} \quad (273\ \mathrm{K} \le T \le 571\ \mathrm{K}) \quad \text{(VI)}$$

The data are not represented quite as well using the standard Arrhenius expression, although one could argue that given the scatter in the data, an Arrhenius fit is satisfactory. The best fit Arrhenius expression,

$$k_{1a}(T) = (2.7 \pm 0.5) \times 10^{-11} \exp[-(201 \pm 77)/T]\ \mathrm{cm^3\ molecule^{-1}\ s^{-1}} \quad (273\ \mathrm{K} \le T \le 571\ \mathrm{K}) \quad \text{(VII)}$$

is plotted as a dotted line in Figure 4. Uncertainties in expression VII are 2σ and represent the precision of the Arrhenius parameters only. The solid line in Figure 4 supports the assumption of a temperature-independent value of k_{1a} that was used to estimate k_{1a}/k_1 values under the conditions of the Martinez et al.[34] and Riffault et al.[35] studies (273−335 K).

Kinetics at T = 330 K. At temperatures intermediate between the low-temperature regime (T < 300 K) and the high-temperature regime (T > 430 K), regeneration of Cl atoms via a secondary reaction became evident. Under these experimental conditions, observed Cl atom temporal profiles were independent of laser fluence and Cl_2CO concentration but varied as a function DMSO concentration, pressure, and temperature in the manner expected if unimolecular decomposition of the Cl−DMSO adduct was the source of regenerated chlorine atoms. Hence, the complete kinetic scheme for describing chlorine atom kinetics in the intermediate temperature regime includes not only reactions 1a, 1b, and 3 but also reactions −1b and 4:

$$CH_3(Cl)S(O)CH_3 + M \rightarrow Cl + CH_3S(O)CH_3 + M \quad (-1b)$$

$$CH_3(Cl)S(O)CH_3 \rightarrow \text{loss via processes that do not generate Cl atoms} \quad (4)$$

Assuming that all processes affecting the temporal evolution of Cl and Cl−DMSO are first-order or pseudo-first-order, the rate equations for the above reaction scheme can be solved analytically:

$$S_t = S_0\{(Q + a)\exp(at) - (Q + b)\exp(bt)\}(a - b)^{-1} \quad \text{(VIII)}$$

In eq VIII, S_t and S_0 are the resonance fluorescence signal levels at times t and 0 (the laser fires at time = 0), and

$$Q = k_{-1b} + k_4 \quad \text{(IX)}$$

$$Q + k_3 + (k_{1a} + k_{1b})[\mathrm{DMSO}] = -(a + b) \quad \text{(X)}$$

$$Q(k_3 + k_{1a}[\mathrm{DMSO}]) + k_4 k_{1b}[\mathrm{DMSO}] = ab \quad \text{(XI)}$$

Observed resonance fluorescence temporal profiles were fit to the double exponential eq VIII using a nonlinear least-squares method to obtain values for a, b, Q, and S_0. The background Cl atom loss rate (k_3) was directly measured and the 330 K rate coefficient for the pressure-independent reaction (k_{1a}) was taken to be 1.44 × 10^{-11} cm^3 $molecule^{-1}$ s^{-1} on the basis of the data shown in Figure 4. Rearrangement of the above equations shows that the rate coefficients k_{1b}, k_{-1b}, and k_4 can be obtained from the fit parameters and the experimental values for k_3 and k_{1a} using the following relationships:

$$k_{1b} = -(Q + k_3 + k_{1a}[\mathrm{DMSO}] + a + b)[\mathrm{DMSO}]^{-1} \quad \text{(XII)}$$

$$k_4 = \{ab - Q(k_3 + k_{1a}[\mathrm{DMSO}])\}(k_{1b}[\mathrm{DMSO}])^{-1} \quad \text{(XIII)}$$

$$k_{-1b} = Q - k_4 \quad \text{(XIV)}$$

As a result of limitations imposed by the relatively fast hydrogen transfer reaction, the strong dependence of k_{-1b} on temperature, the range of experimentally accessible reaction times, and the

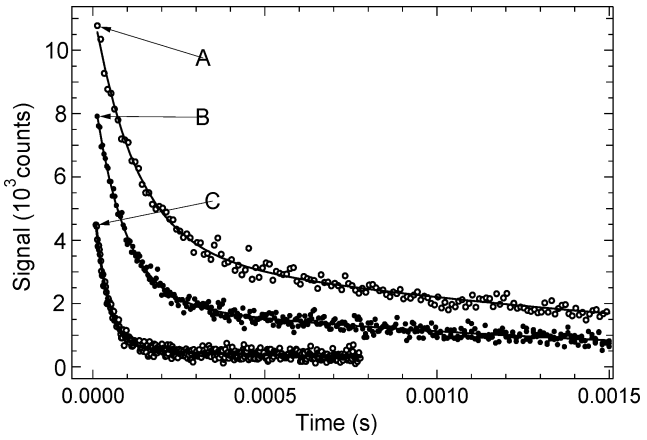

Figure 5. Typical Cl atom temporal profiles (S_t vs time) observed at $T = 330$ K and $P = 280$ Torr. Other experimental conditions: $[Cl_2CO] = (4.4-5.1) \times 10^{14}$ molecules cm^{-3}; $[Cl]_{t=0} = (8-9) \times 10^{11}$ atoms cm^{-3}; [DMSO] in units of 10^{13} molecules cm^{-3} = (a) 6.31, (b) 10.6, and (c) 29.0. Solid lines are obtained from nonlinear least-squares fits to eq VIII. The best fit parameters *a*, *b*, and *Q* are summarized in Table 2.

reduction in signal levels with increasing nitrogen pressure, data of sufficient quality to allow quantitative evaluation of both k_{1b} and k_{-1b} from the analysis described above could only be obtained over a fairly narrow range of temperatures and pressures. As a result, we focused a majority of our effort on one set of conditions, $T = 330$ K and $P = 280$ Torr. Some variations in T and P were carried out to demonstrate that (qualitatively) the expected behavior was observed, but the quantitative analysis has been restricted to the 330 K, 280 Torr data. Typical Cl atom temporal profiles obtained at $T = 330$ K and $P = 280$ Torr are shown in Figure 5 along with the best fits of each temporal profile to eq VIII. The results obtained from quantitative analysis of 10 temporal profiles spanning almost a factor of 6 variation in [DMSO] are summarized in Table 2. It is worth noting that values for k_{1b} obtained from analysis of the double exponential decays are consistent with those obtained at lower temperatures where chlorine atom regeneration was negligibly slow. Although there is a slight tendency for the derived value of k_{1b} to decrease with increasing DMSO concentration, we believe that the mean value of k_{1b} obtained from the data in Table 2, 7.16 x 10^{-11} cm^3 molecule^{-1} s^{-1}, is accurate to ±30%. The precision of the values for k_{-1b} reported in Table 2 is also quite good, although in this case there is a slight tendency for the derived value of k_{-1b} to increase with increasing DMSO concentration. We estimate that the mean value for k_{-1b} obtained from the data in Table 2, 2920 s^{-1}, is also accurate to within ±30%. Also given in Table 3 are values for K_p that are derived from the following relationship:

$$K_p = k_{1b}(k_{-1b}RT)^{-1} = K_c(RT)^{-1} \qquad \text{(XV)}$$

The accuracy of the average value for K_p obtained from the data in Table 3, 5.60 × 10^5 atm^{-1}, is estimated to be ±40% at the 95% confidence level.

Possible Secondary Chemistry Complications. The photochemical system used to study the kinetics of reactions 1a, 1b, and −1b appears to be relatively free of complications from unwanted side reactions. The high purity of the DMSO sample (>99.9%) coupled with the fact that the reactions under investigation are quite fast rules out significant Cl atom loss via reaction with impurities in the DMSO. Radical−radical interactions such as reactions 5 and 6 are not expected to contribute significantly to Cl atom removal because of the reasonably low radical concentrations employed, i.e., usually less than 1×10^{12} per cm^3, and the relatively short time scales for kinetic observations (Cl atom lifetimes in experiments with DMSO present were typically in the range 30−500 μs).

$$Cl + CH_3S(O)CH_2 \rightarrow \text{products} \qquad (5)$$

$$Cl + CH_3(Cl)S(O)CH_3 \rightarrow \text{products} \qquad (6)$$

Even if reactions 5 and 6 occurred on every reactant encounter, these processes would not be fast enough to compete with reaction 1 as a Cl atom removal pathway under the experimental conditions employed. Experimentally, the fact that observed kinetics were unaffected by factors of 3 variation in $[Cl]_0$ (see Table 1) confirms that reactions 5 and 6 were unimportant Cl atom removal mechanisms.

Interaction of the radical products of the Cl + DMSO reaction with phosgene is a chlorine atom regeneration mechanism that warrants consideration:

$$CH_3S(O)CH_2 + Cl_2CO \rightarrow CH_3S(O)CH_2Cl + ClCO \qquad (7)$$

$$CH_3(Cl)S(O)CH_3 + Cl_2CO \rightarrow CH_3S(O)CH_3 + Cl_2 + ClCO \qquad (8)$$

$$ClCO + M \rightarrow Cl + CO + M \qquad (9)$$

Because ClCO is bound by only 32 kJ mol^{-1},[51] reaction 9 would occur very rapidly following ClCO generation via reactions 7 or 8. Based on the enthalpy of formation of Cl−DMSO determined in this study (see below), reaction 8 is very endothermic and cannot be fast enough to represent a significant source of regenerated Cl atoms. The enthalpies of formation of $CH_3S(O)CH_2$ and $CH_3S(O)CH_2Cl$ are not well established. However, based on the known thermochemistry of the analogous reaction that generates CH_3SCH_2Cl from CH_3SCH_2,[52−55] it seems likely that reaction 7 is energetically favorable. Furthermore, theoretical calculations carried out as part of this study and elsewhere[56] allow us to estimate that the 298 K heats of formation of $CH_3S(O)CH_2$ and $CH_3S(O)CH_2Cl$ are +62 ± 10 and −167 ± 10 kJ mol^{-1}, respectively; in conjunction with the known heats of formation of ClCO[51] and Cl_2CO,[45] these theoretical estimates lead to an estimated value of −31 ± 24 kJ mol^{-1} for $\Delta_rH°$ for reaction 7. Experimentally, internally consistent results were obtained over a factor of 5 range of Cl_2-CO concentrations (see Table 1), thus confirming that even though reaction 7 appears to be exothermic, it is too slow to significantly affect the Cl time history under the experimental conditions employed.

Ab Initio Calculations. All calculations were made with Gaussian 98.[57] Optimized geometries were determined using density functional theory[58] with the B3LYP exchange/correlation functional[59] and using MP2. In the DFT calculations, the 6-31+G(d) basis set was used for all atoms except bromine where an effective core potential (ECP(S))[60] was used for the core electrons in conjunction with a 311/311/1 basis set contraction for the valence orbitals. The G2(MP2) level of theory[61] (with MP2/6-31+G(d) geometries and frequencies) was used to calculate the binding enthalpy of Cl with DMS and DMSO. For the G2(MP2) binding enthalpy of Br with DMS and DMSO, MP2 geometries and frequencies were determined with the 6-31+G(d) basis set for all atoms except bromine where the ECP(S) effective core potential was used.[62,63] For the G2(MP2) binding enthalpy of OH with DMS and DMSO, the MP2/6-31+G(2d) level was used to compute geometries and

TABLE 3: Calculated Binding Enthalpies (kJ mol^{-1}) at 0 K and (298 K) for Cl, Br, and OH Adducts with DMS and DMSO

	X−DMS			X−DMSO		
	X = Cl	X = Br	X = OH	X = Cl	X = Br	X = OH
PMP2/3-21+G(d)[a]	51.0	50.6		31.0	44.8	
[QCISD(T)/6-31+G(2d,p)]//UMP2/6-31+G(2d)[a]			36.4			
B3LYP/6-31+G(d)/ECP(Br)[b,c]	90.0	87.4	(47.3)	77.4	77.0	(49.4)
B3LYP/6-311+G(2df,p)//B3LYP/6-311+G(d,p)[d]	(97.0)					
UQCISD(T)//UMP2/DZP[e]	(53.2)					
G2(MP2)[f]	78.9 (80.4)	47.0 (48.2)	43.6 (46.7)	64.8 (66.1)	30.4 (31.4)	49.1 (55.0)
G3B3[g,h]	80.8 (81.8)	62.7 (63.4)		65.8 (66.6)	44.7 (45.2)	
G3//MP2/6-311G(d,p)[i]						46.6 (50.7)
QCISD(T)/6-311++G(2df,2p)[j]	74.0	59.0				
CCSD(T)/CBS[k]				71.9 (73.3)		
WF-1[l]			(36.4)			
CCSD(T)/aug-cc-pV(T+d)Z[m]			44.6			
G3S/3//MPW1K//MG3S[n]			(41.4)			

[a] Reference 64. [b] ECP(Br) indicates that an effective core potential was used for bromine. [c] Reference 92. [d] Reference 93. [e] Reference 94. [f] This work. The following varieties of G2(MP2) were used: Cl = G2(MP2)//MP2/6-31+G(d), Br = G2(MP2)[ECP(S)]//MP2/6-31+G(d), OH = G2(MP2)//MP2/6-31+G(2d). [g] This work. For G3B3 method, see Reference 95. [h] For bromine and bromine-containing compounds, the G3B3 method was used with geometries, frequencies (unscaled), and heat capacity corrections from B3LYP/6-31+G(d). See refs 74, 75, and 95. [i] Reference 56. [j] Reference 96. [k] Reference 36. [l] Reference 97. [m] Reference 98. [n] Reference 99. The authors have computed the binding enthalpy (298K) of DMS−OH at twenty different levels of theory.

TABLE 4: Summary of Parameters Used in Calculations of Absolute Entropies and Heat Capacity Corrections

	Cl	$CH_3S(O)CH_3$	$CH_3(Cl)S(O)CH_3$
g_0	4	1	2
g_1	2		
$\Delta\epsilon$ (cm^{-1})[a]	882.36		
rot. constants (cm^{-1})		0.229, 0.228, 0.138	0.143, 0.0633, 0.0608
vib frequencies (cm^{-1})		3226, 3225, 3213	3254, 3251, 3234
		3210, 3101, 3100	3233, 3117, 3117
		1518, 1501, 1497	1505, 1490, 1489
		1483, 1413, 1392	1477, 1411, 1391
		1104, 1073, 1002	1162, 1076, 1021
		977, 942, 730	992, 959, 770
		697, 375, 311	696, 365, 324
		297, 244,[b] 186 [b]	287, 263, 216[b]
			196,[b] 125, 111

[a] $\Delta\epsilon \equiv$ energy splitting between the lowest two electronic states; DMSO has no low-energy excited states and the Cl−DMSO adduct is assumed to have none. [b] Torsional frequencies which are treated as vibrations in the entropy calculation (see text).

frequencies due to the inability of the MP2/6-31+G(d) level to correctly describe the 2c−3e interaction between OH and DMS.[64] In addition, G3B3 calculations[65] (based on B3LYP/6-31G(d) geometries and frequencies) were made for the binding enthalpy of Cl with DMS and DMSO. Corrections for basis set superposition error[66] (BSSE), which have not been made, might decrease the binding enthalpy by a few kJ/mol.

Reported theoretical X−DMSO and X−DMS binding enthalpies at 0 and 298 K are summarized in Table 3 for X = Cl, Br, and OH. Because density functional theory is known to be defective in describing the spin/charge localization in 2 center−3 electron (2c−3e) bonded systems,[67−74] we believe the G3B3 values to be more reliable than the full DFT results. Interestingly, the G2(MP2) and G3B3 binding enthalpies for Cl−DMS and Cl−DMSO are not sensitive to whether the geometry was optimized at MP2 (G2(MP2)) or DFT (G3B3). For bromine-containing complexes, the G3 method[65,75,76] (adapted for B3LYP/6-31+G(d) geometries, i.e., G3B3) gives binding enthalpies in much better agreement with experiment than the G2(MP2) method (experimental results are summarized in Table 6 and discussed in more detail below).

The B3LYP/6-31+G(d) calculated structures of DMSO and Cl−DMSO are presented in Figure 6. The structure of DMSO obtained from microwave spectroscopy[77] is compared with the calculated structure in Figure 6.

Adduct Thermochemistry. The experimental value for K_p at 330 K (5.6 ± 2.2) × 10^5 atm^{-1}, has been employed in conjunction with a calculated entropy change for reaction 1b to determine the enthalpy change associated with adduct formation:

TABLE 5: Thermochemical Parameters for the Reaction Cl + $CH_3S(O)CH_3$ → $CH_3(Cl)S(O)CH_3$[a,b]

T	$\Delta_rS°$	$\Delta_rH°$	$\Delta_fH°$(Cl−DMSO)[c]
330	−110.5 ± 4.0	−72.8 ± 2.8	
298	−110.6 ± 4.0	−72.8 ± 2.9	−102.7 ± 4.9
0		−71.5 ± 3.3	−84.4 ± 5.8

[a] Units: T (K); $\Delta_rS°$ (J K^{-1} mol^{-1}); $\Delta_rH°$, $\Delta_fH°$(Cl−DMSO) (kJ mol^{-1}). [b] Uncertainties are accuracy estimates at the 95% confidence level. [c] Evaluated assuming the following values for $\Delta_fH°$(X) in units of kJ mol^{-1} (X = Cl or DMSO): +119.6 for Cl at 0 K; +121.3 for Cl at 298 K; −132.5 ± 2.5 for DMSO at 0 K; −151.2 ± 2.0 for DMSO at 298 K. Values for Cl are obtained from ref 78, and values for DMSO are averages of values reported in refs 79−81.

$$\Delta_rH° = T\Delta_rS° - RT\ln K_p \qquad \text{(XVI)}$$

To evaluate $\Delta_rS°$ for reaction 1b, absolute entropies as a function of temperature were obtained from the JANAF tables[78] for Cl, and calculated using ab initio vibrational frequencies and moments of inertia for DMSO and Cl−DMSO. Relevant parameters used in the calculations of absolute entropies and heat capacity corrections are summarized in Table 4. The two lowest frequency normal modes for DMSO (186 and 244 cm^{-1}) and the third and fourth lowest frequency normal modes for

TABLE 6: Comparison of Experimental H-Transfer Rate Coefficients, Addition Rate Coefficients, and Adduct Bond Strengths (All at 298 K) for Reactions of Cl, Br, and OH with DMS and DMSO[a]

reaction	H-transfer rate coefficient[b]	addition rate coefficient[b] 100 Torr[c]	addition rate coefficient[b] 760 Torr[c]	298 K adduct bond strength[d]
Cl + DMS	1800[e] 700 [f]	900[e]	1500[e]	
Br + DMS	0.3[g]	500[h,i,j]	1000[i]	56[i,j]
OH + DMS	50[k,l,m,n,o]	60[l,o,p,q,r,]	200[l,o,p,q,r,]	44[o,p]
Cl + DMSO	145[s,t,TW]	690[TW]	970[TW]	73[TW]
Br + DMSO	*u*			
OH + DMSO	<30[v,w]	900[v,w,x]	900[v,w,x]	

[a] TW ≡ this work. [b] Units are 10^{-13} cm^3 molecule^{-1} s^{-1}. [c] Nitrogen or air bath gas. [d] Units are kJ mol^{-1}; uncertainties are typically ±10 kJ mol^{-1}. [e] Reference 37. [f] Reference 100. [g] Reference 54. [h] Reference 23. [i] Reference 101. [j] Reference 102. [k] Reference 103. [l] Reference 104. [m] Reference 105. [n] Reference 106. [o] Reference 107. [p] Reference 108. [q] Reference 109. [r] Reference 110. [s] Reference 34. [t] Reference 35. [u] Reaction is significantly endothermic and, therefore, very slow. [v] Reference 26. [w] Reference 28. [x] Reference 25.

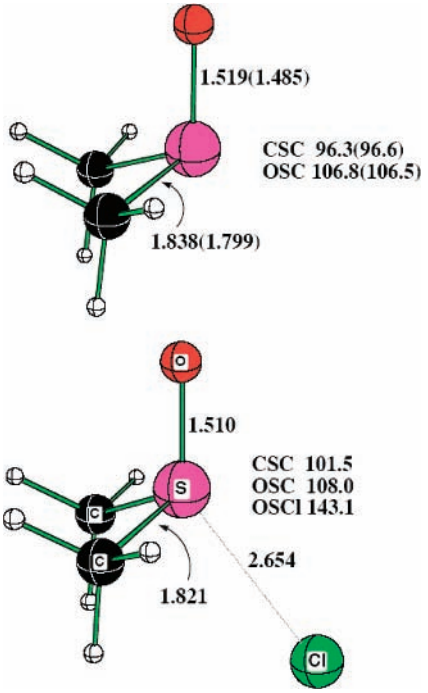

Figure 6. Structures for $CH_3S(O)CH_3$ and $CH_3(Cl)S(O)CH_3$ at the B3LYP/6-31+G(d) level of theory. Bond lengths and bond angles shown in parentheses are experimental values taken from ref 77.

Cl−DMSO (196 and 216 cm^{-1}) are methyl group internal rotations. Some additional calculations, carried out to assess the magnitude of the barriers for CH_3 internal rotations, suggest that these barriers are in the range 5−9 kJ mol^{-1} and are similar enough in magnitude in DMSO and Cl−DMSO that whether these modes are treated as vibrations or hindered rotations has little effect on the calculated value for $\Delta_rS°$; i.e., results differ by <1 J K^{-1} mol^{-1}. At 330 K, our analysis gives the results $\Delta_rS° = -110.5 \pm 4.0$ J K^{-1} mol^{-1} (calculated treating the torsional modes as vibrations) and $\Delta_rH° = -72.8 \pm 2.8$ kJ mol^{-1}; the uncertainties we report reflect an estimate of our imperfect knowledge of the input data needed to calculate absolute entropies (particularly the low-frequency Cl−DMSO vibrations) as well as the estimated uncertainty in the experimental value for K_p(330 K). Appropriate heat capacity corrections have been employed to obtain $\Delta_rH°$ values at 298 and 0 K; the results are given in Table 5. The values for $\Delta_rH°$ in Table 5 can be used in conjunction with literature values for the standard enthalpies of formation of Cl[78] and DMSO[79−81] to deduce values for the standard enthalpy of formation of Cl−DMSO, $\Delta_fH°$(Cl−DMSO), at 298 and 0 K; these values are also given in Table 5.

For comparison with the experimental values for the S−Cl bond strength in Cl−DMSO (see $\Delta_rH°$ values in Table 5), theoretical values have been obtained using density functional theory (DFT) at the B3LYP/6-31+G(d) level and G3B3 theory. Theoretical values for $\Delta_rH°$ at 298 K are as follows:

$$\text{B3LYP/6-31+G(d)} \quad -75.4 \text{ kJ mol}^{-1}$$

$$\text{G3B3} \quad -66.6 \text{ kJ mol}^{-1}$$

The theoretical $\Delta_rH°$ values bracket the experimental value of -72.8 ± 2.9 kJ mol^{-1}, with density functional theory predicting a stronger bond than observation and G3B3 theory predicting a weaker bond; this trend in comparing experimental bond strengths with theoretical bond strengths is also evident in our earlier studies of the CH_3I−Cl,[38] CH_3Br−Cl,[39] and C_2D_5I−Cl[82] adducts. The theoretical bond strengths reported in this study agree quite well with the bond strength obtained by Vandresen and Resende at the CCSD(T)/CBS level of theory. Overall, the agreement between experiment and theory is excellent.

Comparison with Previous Research. As mentioned in the Introduction, four previous studies of Cl + DMSO reaction kinetics are reported in the literature.[24,27,34,35] The results of the low-pressure discharge flow studies of Martinez et al.[34] and Riffault et al.[35] are consistent with the higher pressure data reported in this study and are used in our analysis to derive Arrhenius parameters for reaction 1a and falloff parameters for reaction 1b at room temperature (see Figures 3 and 4 as well as associated discussion). Barnes et al.[24] and Falbe-Hansen et al.[27] both carried out relative rate studies in large (~500 L) chambers at atmospheric pressure and room temperature in air using 254 nm photolysis of Cl_2CO as the photolytic source of chlorine atoms and FTIR spectroscopy to monitor the loss of reactants and the formation of products. The rate coefficients reported in the two studies, in units of 10^{-11} cm^3 molecule^{-1} s^{-1}, are 7.4 ± 1.8[24] and 7.4 ± 1.0,[27] where the uncertainties represent 1σ, precision only[24] and 2σ, overall uncertainty,[27] respectively. Significant heterogeneous loss of DMSO, i.e., 20−40% of the gas-phase loss rate, was observed in both studies. Barnes et al.[24] also carried out experiments in N_2 bath gas and obtained the somewhat slower rate coefficient $(5.4 \pm 1.4) \times 10^{-11}$ cm^3 molecule^{-1} s^{-1}, where the uncertainty is 1σ, precision only. Sulfur dioxide (SO_2) and dimethyl sulfone ($CH_3(O)S(O)CH_3$, DMSO2) were observed as end products in both studies. The rate coefficients reported in the relative rate studies are factors of 1.5−2 slower than the rate coefficients we obtain at room temperature and pressures approaching 1 atm, although it should be kept in mind that uncertainties in all reported rate coefficients (including those reported in this study) are substantial because of the problems associated with handling DMSO in the gas phase. One possible explanation why slower rate coefficients are measured in the relative rate studies concerns the fact that secondary conversion of the adduct into DMSO via reaction −1b, via adduct photolysis, or via the adduct self-reaction,

$$2CH_3(Cl)S(O)CH_3 \rightarrow 2CH_3S(O)CH_3 + Cl_2 \qquad (10)$$

would not be observed as a reaction in the relative rate studies; i.e., we measure the total rate coefficient for adduct formation

whereas the relative rate studies only measure the fraction of addition events for which the adduct is not converted back to DMSO. The slower rate coefficient measured by Barnes et al.[24] in 1 atm N_2 compared to the one measured in 1 atm air could be rationalized as resulting from an adduct + O_2 reaction that is fast enough to compete with reactions −1b and 10 for adduct removal. In a recent conference presentation, Wine et al.[83] report an upper limit of 1×10^{-18} cm^3 molecule^{-1} s^{-1} for the Cl−DMSO + O_2 rate coefficient, but the reported upper limit does not rule out the importance of Cl−DMSO + O_2 in the Barnes et al. study. In another recent conference presentation, Arsene et al.[84] report relative rate studies of the Cl + DMSO reaction in 1 atm N_2+O_2 as a function of temperature (283−308 K) and O_2 partial pressure (0−500 mbar). The rate coefficients reported by Arsene et al.[84] are extremely fast, i.e., $(2.2-3.6) \times 10^{-10}$ cm^3 molecule^{-1} s^{-1}, increase with increasing temperature, and are independent of O_2 partial pressure. The magnitude of the rate coefficients reported by Arsene et al. seem inconsistent with those obtained in this study, and both the magnitude of the rate coefficients and the lack of a dependence on O_2 partial pressure are inconsistent with the results of Barnes et al.[24] The results of Barnes et al. and Arsene et al. have not been published in the peer-reviewed literature, so additional relative rate studies that pay careful attention to quantifying heterogeneous DMSO loss processes and other potential secondary chemistry complications would be desirable. It is worth pointing out that the occurrence of reaction 10 in the Arsene et al. study could explain the rapid DMSO removal observed by these investigators, because DMSO is known to react with Cl_2, a product of reaction 10. As discussed above in the context of other radical−radical reactions, the time scale of our experiment and the low concentrations of Cl−DMSO present in our laser flash photolysis reactor rule out significant impact on observed Cl kinetics in our study from either reaction 10 or a subsequent DMSO + Cl_2 reaction.

The results reported in this paper for the Cl + DMSO reaction have been combined with other available information to construct Table 6, a comparison of *experimental* H-transfer rate coefficients, addition rate coefficients, and adduct bond strengths for reactions of Cl, Br, and OH with DMS and DMSO. All of the quantities tabulated in Table 6 except for the OH + DMS H-transfer rate coefficient have significant uncertainties, but the numbers, which represent our best estimates based on available information, allow some interesting qualitative comparisons.

The reactivity of the radical species toward H-transfer follows the trend Cl > OH > Br which is typical of many radical + organic reactions.[85] The C−H bonds in DMS and DMSO are strong enough that the Br + DMS H-transfer reaction is slightly endothermic[54] and the corresponding Br + DMSO reaction is significantly endothermic. The upper limit of 3.0×10^{-12} cm^3 molecule^{-1} s^{-1} for the OH + DMSO H-transfer reaction is consistent with experimental data that demonstrate a high yield for production of CH_3 + $CH_3S(O)OH$ from the OH + DMSO reaction.[26,28,86]

Based on a combination of experimental and theoretical work (see Tables 3 and 6 for references), the bond strengths for all adducts of interest except Br−DMSO appear to be known to within about ±10 kJ mol^{-1}). Because there are no data in the literature concerning the stability of Br−DMSO, we have carried out electronic structure calculations for this adduct that are analogous to those described above for Cl−DMSO. The following results are obtained for $\Delta_r H°$ for the Br + DMSO association reaction at 298 K:

B3LYP/6-31+G(d)	−63.6 kJ mol^{-1}
G3B3	−45.2 kJ mol^{-1}

The difference in the adduct bond strengths calculated by the two methods is substantially larger than the corresponding difference in the Cl + DMSO calculations (see above). This difference is likely a result of the fact that the 2c−3e interaction in Cl−DMSO is more symmetrical than the corresponding interaction in Br−DMSO; i.e., the unpaired spin density is more evenly distributed between Cl and S in Cl−DMSO (0.50/0.24) than between Br and S in Br−DMSO (0.11/0.69). Hence, the large difference between G3B3 and DFT for Br−DMSO can likely be attributed to the known failure of DFT to properly describe unsymmetrical 2c−3e systems. The only published experimental study of Br + DMSO kinetics is a recent chamber study by Ballesteros et al.[87] These investigators employed continuous photolysis with FTIR detection of reactants and products; they carried out their study at room temperature and atmospheric pressure of air bath gas. Ballesteros et al. found the Br + DMSO reaction to be very slow, i.e., $k < 1 \times 10^{-15}$ cm^3 molecule^{-1} s^{-1}, suggesting that if an adduct is formed, it decomposes back to reactants on a time scale that is fast compared to the time scale for other competing processes such as reaction with O_2, photolysis to products other than Br + DMSO, or radical−radical reactions.

The information summarized in Tables 3 and 6 indicates that Cl forms more strongly bound adducts than Br with DMS and DMSO, and also that Cl atoms form a more strongly bound adduct with DMS than with DMSO. The 2c−3e bond strength for neutral complexes is strongest when the HOMO orbital energy of the closed-shell fragment best matches the SOMO orbital energy of the radical fragment.[88] The orbital energy match can be related to the difference in the ionization energy (IE) of the closed-shell fragment and the electron affinity (EA) of the radical fragment. A smaller difference results in a larger binding enthalpy. For the Cl−DMS complex, the orbital energy match is nearly optimal which results in a very strong 2c−3e bond enthalpy. The orbital match is slightly worse in the Cl−DMSO complex and the binding enthalpy is somewhat smaller. In the Br−DMS and Br−DMSO complexes, the smaller IE of Br relative to Cl (7.88 eV compared to 8.80 eV) leads to a poorer orbital match and a weaker 2c−3e interaction. In the Br−DMSO complex, the small unpaired spin density on Br (0.11) indicates that donor−acceptor interactions are becoming important. Opposite to the trend observed for Cl adducts (and probably also for Br adducts), the OH−DMSO adduct appears to be more strongly bound than the OH−DMS adduct. Wang and Zhang[56] suggest that hydrogen bonding between OH and the O atom in DMSO is the reason that the OH−DMSO adduct is more strongly bound than the OH−DMS adduct. Alternatively, the difference in ionization potentials between DMSO and DMS may provide a better orbital match in the OH−DMSO case.

Implications for Atmospheric Chemistry. The two most important removal processes for atmospheric DMSO(g) are widely accepted to be reaction with OH and uptake into the condensed phase. Assuming an average OH concentration of 9×10^5 molecules cm^{-3} [89] and an OH + DMSO rate coefficient of 9×10^{-11} cm^3 molecule^{-1} s^{-1},[25,26,28] suggests an average DMSO lifetime of 3 h toward reaction with OH. DMSO lifetimes of 1−10 h toward uptake into the condensed phase have been inferred from field observations.[90] Estimation of an average lifetime for DMSO loss via reaction with Cl atoms is difficult because of (a) the temporal and spatial variability of atmospheric Cl concentrations and (b) the uncertain atmospheric

fate of Cl−DMSO. Assuming an average Cl concentration of 4×10^4 atoms cm^{-3}, which appears to be appropriate for the marine boundary layer (MBL),[91] and no regeneration of DMSO from Cl−DMSO, one obtains a lifetime of 60 h for DMSO removal by reaction with Cl. In the other limiting scenario where all Cl−DMSO is converted back to DMSO, the DMSO lifetime toward removal by Cl would be about 460 h. Hence, it appears that reaction with Cl accounts for 0.3−6% of MBL DMSO removal, depending on the amount of aerosol loading and on the ultimate fate of Cl−DMSO under atmospheric conditions.

Acknowledgment. This research was supported by the National Science Foundation through grants ATM-99-10912 and ATM-03-50185 to Georgia Institute of Technology. Computer time for this study was made available by the Alabama Supercomputer Network, the Maui High Performance Computing Center, and the Auburn COSAM PRISM cluster.

References and Notes

(1) Davis, D.; Chen, G.; Kasibhatla, P.; Jefferson, A.; Tanner, D.; Eisele, F.; Lenschow, D.; Neff, W.; Berresheim, H. *J. Geophys. Res.* **1998**, *103*, 1657.

(2) Nowak, J. B.; Davis, D. D.; Chen, G.; Eisele, F. L.; Mauldin, R. L.; Tanner, D. J.; Cantrell, C.; Kosciuch, E.; Bandy, A.; Thornton, D.; Clarke, A. *Geophys. Res. Lett.* **2001**, *28*, 2201.

(3) Barnes, I.; Becker, K. H.; Patroescu, I. *Geophys. Res. Lett.* **1994**, *21*, 2389.

(4) Barnes, I.; Becker, K. H.; Patroescu, I. *Atmos. Environ.* **1996**, *30*, 1805.

(5) Sorensen, S.; Falbe-Hansen, H.; Mangoni, M.; Hjorth, J.; Jensen, N. R. *J. Atmos. Chem.* **1996**, *24*, 299.

(6) Arsene, C.; Barnes, I.; Becker, K. H. *Phys. Chem. Chem. Phys.* **1999**, *1*, 5463.

(7) Arsene, C.; Barnes, I.; Becker, K. H.; Mocanu, R. *Atmos. Environ.* **2001**, *35*, 3769.

(8) Bates, T. S.; Lamb, B. K.; Guenther, A.; Dignon, J.; Stoiber, R. E.; *J. Atmos. Chem.* **1992**, *14*, 315.

(9) Spiro, P. A.; Jacob, D. J.; Logan, J. A. *J. Geophys. Res.* **1992**, *97*, 6023.

(10) Berresheim, H.; Wine, P. H.; Davis, D. D. In *Composition, Chemistry, and Climate of the Atmosphere*; Singh, H. B., Ed.; Van Nostrand Reinhold: New York, 1995; pp 251−307.

(11) Watts, S. F. *Atmos. Environ.* **2000**, *34*, 761.

(12) Charlson, R. J.; Lovelock, J. E.; Andreae, M. O.; Warren, S. G. *Nature* **1987**, *326*, 655.

(13) Pirjola, L.; O'Dowd, C. D.; Brooks, I. M.; Kulmala, M. *J. Geophys. Res.* **2000**, *105*, 26531.

(14) Yoon, Y. J.; Brimblecombe, P. *Atmos. Chem. Phys.* **2002**, *2*, 17.

(15) Boucher, O.; Moulin, C.; Belviso, S.; Aumont, O.; Bopp, L.; Cosme, E.; von Kuhlmann, R.; Lawrence, M. G.; Pham, M.; Reddy, M. S.; Sciare, J.; Venkataraman, C. *Atmos. Chem. Phys.* **2003**, *3*, 49.

(16) IPCC, 2001: *Climate Change 2001: The Scientific Basis. Contribution of Working Group I to the Third Assessment Report of the Intergovernmental Panel on Climate Change*; Houghton, J. T., Ding, Y., Griggs, D. J., Noguer, M., van der Linden, P. J., Dai, X., Maskell, K., Johnson, C. A., Eds.; Cambridge University Press: Cambridge, U.K., and New York, 2001; 881 pp.

(17) Ayres, G. P.; Cainey, J. M.; Gillett, R. W.; Ivey, J. P. *Philos. Trans. R. Soc. London B* **1997**, *352*, 203.

(18) Lucas, D. D.; Prinn, R. G. *J. Geophys. Res.* **2002**, *107* (D14), 4201, 10.1029/2001JD000843.

(19) Hynes, A. J.; Stickel, R. E.; Pounds, A. J.; Zhao, Z.; McKay, T.; Bradshaw, J. D.; Wine, P. H. In *Dimethyl sulfide: Oceans, Atmosphere, and Climate*; Restelli, G., Angelletti, G., Eds.; Kluwer: Dordrecht, The Netherlands, 1993; pp 211−221.

(20) Turnipseed, A. A.; Barone, S. B.; Ravishankara, A. R. *J. Phys. Chem.* **1996**, *100*, 14703.

(21) Barnes, I.; Bastian, V.; Becker, K. H.; Overath, R. *Int. J. Chem. Kinet.* **1991**, *23*, 579.

(22) Bedjanian, Y.; Poulet, G.; LeBras, G. *Int. J. Chem. Kinet.* **1996**, *28*, 383.

(23) Ingham, T.; Bauer, D.; Sander, R.; Crutzen, P. J.; Crowley, J. N. *J. Phys. Chem. A* **1999**, *103*, 7199.

(24) Barnes, I.; Bastian, V.; Becker, K. H.; Martin, D. In *Biogenic Sulfur in the Environment*; Saltzman, E. S., Cooper, W. J., Eds.; ACS Symp. Ser. No. 393; American Chemical Society: Washington, DC, 1989; pp 476−488.

(25) Hynes, A. J.; Wine, P. H. *J. Atmos. Chem.* **1996**, *24*, 23.

(26) Urbanski, S. P.; Stickel, R. E.; Wine, P. H. *J. Phys. Chem. A* **1998**, *102*, 10522.

(27) Falbe-Hansen, H.; Sorensen, S.; Jensen, N. R.; Pedersen, T.; Hjorth, J. *Atmos. Environ.* **2000**, *34*, 1543.

(28) Kukui, A.; Borissenko, D.; Laverdet, G.; LeBras, G. *J. Phys. Chem. A* **2003**, *107*, 5732.

(29) Davis, D.; Chen, G.; Bandy, A.; Thornton, D.; Eisele, F.; Mauldin, L.; Tanner, D.; Lenschow, D.; Fuelberg, H.; Huebert, B.; Heath, J.; Clarke, A.; Blake, D. *J. Geophys. Res.* **1999**, *104*, 5765.

(30) Zhu, L.; Nicovich, J. M.; Wine P. H. *J. Photochem. Photobiol. A: Chem.* **2003**, *157*, 311.

(31) Zhu, L.; Nicovich, J. M.; Wine, P. H. *Aquat. Sci.* **2003**, *65*, 425.

(32) Zhu, L.; Nicovich, J. M.; Wine, P. H. *J. Phys. Chem. A* **2005**, *109*, 3903.

(33) Zhu, L.; Nenes, A.; Wine, P. H.; Nicovich, J. M. *J. Geophys. Res.*, in press.

(34) Martinez, E.; Aranda, A.; Diaz de Mera, Y., Rodriguez, D.; Lopez, M. R.; Albaladejo, J. *Environ. Sci. Technol.* **2002**, *36*, 1226.

(35) Riffault, V.; Bedjanian, Y.; Le Bras, G. *Phys. Chem. Chem. Phys.* **2003**, *5*, 2828.

(36) Vandresen, S.; Resende, S. M. *J. Phys. Chem. A* **2004**, *108*, 2284.

(37) Stickel, R. E.; Nicovich, J. M.; Wang, S.; Zhao, Z.; Wine, P. H. *J. Phys. Chem.* **1992**, *26*, 9875.

(38) Nicovich, J. M.; Wang, S.; Wine, P. H. *Int. J. Chem. Kinet.* **1995**, *27*, 359.

(39) Nicovich, J. M.; Wang, S.; McKee, M. L.; Wine, P. H. *J. Phys. Chem.* **1996**, *100*, 680.

(40) Bilde, M.; Sehested, J.; Nielsen, O. J.; Wallington, T. J.; Meagher, R. J.; McIntosh, M. E.; Piety, C. A.; Nicovich, J. M.; Wine, P. H. *J. Phys. Chem. A* **1997**, *101*, 8035.

(41) Ayhens, Y. V.; Nicovich, J. M.; McKee, M. L.; Wine, P. H. *J. Phys. Chem. A* **1997**, *101*, 9382.

(42) Piety, C. A.; Soller, R.; Nicovich, J. M.; McKee, M. L.; Wine, P. H. *Chem. Phys.* **1998**, *231*, 155.

(43) Finlayson-Pitts, B. J.; Pitts, J. N., Jr. *Chemistry of the Upper and Lower Atmosphere*; Academic Press: San Diego, 2000; p 146.

(44) Douglas, T. B. *J. Am. Chem. Soc.* **1948**, *70*, 2001.

(45) Sander, S. P.; Friedl, R. R.; Golden, D. M.; Kurylo, M. J.; Huie, R. E.; Orkin, V. L.; Moortgat, G. K.; Ravishankara, A. R.; Kolb, C. E.; Molina, M. J.; Finlayson-Pitts, B. J. *Chemical Kinetics and Photochemical Data for Use in Atmospheric Studies*; Evaluation No. 14; Jet Propulsion Laboratory Publication 02-25; Jet Propulsion Laboratory: Pasadena, CA, 2003.

(46) Maul, C.; Haas, T.; Gericke, K.-H.; Comes, F. J. *J. Chem. Phys.* **1995**, *102*, 3238.

(47) Chichinin, A. I. *Chem. Phys. Lett.* **1993**, *209*, 459.

(48) Tyndall, G. S.; Orlando, J. J.; Kegley-Owen, C. S. *J. Chem. Soc. Faraday Trans.* **1995**, *91*, 3055.

(49) Fletcher, I. S.; Husain, D. *Chem. Phys. Lett.* **1977**, *49*, 516.

(50) Chichinin, A. I.; Krasnoperov, L. N. *Chem. Phys. Lett.* **1989**, *160*, 448.

(51) Nicovich, J. M.; Kreutter, K. D.; Wine, P. H. *J. Chem. Phys.* **1990**, *92*, 3539.

(52) Chase, M. W. Jr.; Davies, C. A.; Downey, J. R. Jr.; Frurip, D. J.; McDonald, R. A.; Syverud, A. N. *J. Phys. Chem. Ref. Data* **1985**, *14*, Supplement No. 1.

(53) Nourbakhsh, S.; Norwood, K.; Yin, H.-M.; Liao, C.-L.; Ng, C. Y. *J. Chem. Phys.* **1991**, *95*, 5014.

(54) Jefferson, A.; Nicovich, J. M.; Wine, P. H. *J. Phys. Chem.* **1994**, *98*, 7128.

(55) Hynes, A. J.; Wine, P. H. In *Gas-Phase Combustion Chemistry*; Gardiner, W. C., Jr., Ed.; Springer, New York, **2000**; pp 343−388.

(56) Wang, L.; Zhang, J. *Chem. Phys. Lett.* **2002**, *356*, 490.

(57) Frisch, M. J.; Trucks, G. W.; Schlegel, H. B.; Scuseria, G. E.; Robb, M. A.; Cheeseman, J. R.; Zakrzewski, V. G.; Montgomery, J. A., Jr.; Stratmann, R. E.; Burant, J. C.; Dapprich, S.; Millam, J. M.; Daniels, A. D.; Kudin, K. N.; Strain, M. C.; Farkas, O.; Tomasi, J.; Barone, V.; Cossi, M.; Cammi, R.; Mennucci, B.; Pomelli, C.; Adamo, C.; Clifford, S.; Ochterski, J.; Petersson, G. A.; Ayala, P. Y.; Cui, Q.; Morokuma, K.; Malick, D. K.; Rabuck, A. D.; Raghavachari, K.; Foresman, J. B.; Cioslowski, J.; Ortiz, J. V.; Stefanov, B. B.; Liu, G.; Liashenko, A.; Piskorz, P.; Komaromi, I.; Gomperts, R.; Martin, R. L.; Fox, D. J.; Keith, T.; Al-Laham, M. A.; Peng, C. Y.; Nanayakkara, A.; Gonzalez, C.; Challacombe, M.; Gill, P. M. W.; Johnson, B.; Chen, W.; Wong, M. W.; Andres, J. L.; Gonzalez, C.; Head-Gordon, M.; Replogle, E. S.; and Pople, J. A. *Guassian 98*, revision A.6; Gaussian, Inc.: Pittsburgh, PA, 1998.

(58) Koch, W., Holthausen, M. C. *A Chemist's Guide to Density Functional Theory*; Wiley-VCH: New York, 2000.

(59) Becke, A. D. *J. Chem. Phys.* **1993**, *98*, 5648.

(60) The ECP(S) for Br came from: (a) Bergner, A.; Dolg, M.; Küchle, W.; Stoll, H.; Preuss, H. *Mol. Phys.* **1993**, *80*, 1431. (b) Schwerdtfeger, P.;

Dolg, M.; Schwarz, W. H.; Bowmaker, G. A.; Boyd, P. D. W. *J. Chem. Phys.* **1989**, *91*, 1762.

(61) G2(MP2): Curtiss, L. A.; Raghavachari, K.; Pople, J. A. *J. Chem. Phys.* **1993**, *98*, 1293.

(62) Glukhovtsev, M. N.; Pross, A.; McGrath, M. P.; Radom, L. *J. Chem. Phys.* **1995**, *103*, 1878; Erratum. *J. Chem. Phys.* **1996**, *104*, 3407.

(63) (a) Glukhovtsev, M. N.; Pross, A.; Radom, L. *J. Am. Chem. Soc.* **1995**, *117*, 9012. (b) Glukhovtsev, M. N.; Pross, A.; Radom, L. *J. Phys. Chem.* **1996**, *100*, 3498.

(64) McKee, M. L. *J. Phys. Chem.* **1993**, *97*, 10971.

(65) G3B3: Curtiss, L. A.; Redfern, P. C.; Raghavachari, K.; Rassolov, V.; Pople, J. A. *J. Chem. Phys.* **1999**, *110*, 4703.

(66) BSSE: van Duijneveldt, F. B.; van Duijneveldt-van de Rijdt, J. G. C. M.; van Lenthe, J. H. *Chem. Rev.* **1994**, *94*, 1873.

(67) Braïda, B.; Hazebroucq, S.; Hiberty, P. C. *J. Am. Chem. Soc.* **2002**, *124*, 2371.

(68) Chermette, H.; Ciofini, I.; Mariotti, F.; Daul, C. *J. Chem. Phys.* **2001**, *115*, 11068.

(69) Braïda, B.; Lauvergnat, D.; Hiberty, P. C. *J. Chem. Phys.* **2001**, *115*, 90.

(70) Braïda, B.; Hiberty, P. C. *J. Phys. Chem. A* **2000**, *104*, 4618.

(71) Braïda, B.; Thogersen, L.; Wu, W.; Hiberty, P. C. *J. Am. Chem. Soc.* **2002**, *124*, 11781.

(72) Bally, T.; Sastry G. N. *J. Phys. Chem. A* **1997**, *101*, 7923.

(73) Braïda, B.; Hiberty, P. C.; Savin, A. *J. Phys. Chem. A* **1998**, *102*, 7872.

(74) Sodupe, M.; Bertran, J.; Rodriguez-Santiago, L.; Baerends, E. J. *J. Phys. Chem A* **1999**, *103*, 166.

(75) Curtiss, L. A.; Redfern, P. C.; Rassolov, V.; Kedziora, G.; Pople, J. A. *J. Chem. Phys.* **2001**, *114*, 9287.

(76) Curtiss, L. A.; Raghavachari, K.; Redfern, P. C.; Rassolov, V.; Pople, J. A. *J. Chem. Phys.* **1998**, *109*, 7764.

(77) *Structure of Free Polyatomic Molecules*; Landolt-Börnstein, New Series, Vol. 7; Madelung, O., Ed.; Springer-Verlag: New York, 1987.

(78) Chase, M. W., Jr.; Davies, C. A.; Downey, J. R., Jr.; Frurip, D. J.; McDonald, R. A.; Syverud, A. N. *J. Phys. Chem. Ref. Data* **1985**, *14*, Suppl. I.

(79) Lias, S. G.; Bartmess, J. E.; Liebman, J. F.; Holmes, J. L.; Levin, R. D.; Mallard, W. G. *J. Phys. Chem. Ref. Data* **1988**, *17*, Suppl. No. 1.

(80) Masuda, N.; Nagano, Y.; Sakiyama, M. *J. Chem. Thermodyn.* **1994**, *26*, 971.

(81) Theoretical heats of formation calculated using G3B3 theory. See http://chemistry.anl.gov/compmat/g3xenergies/G3SXHeatsofFormation.htm.

(82) Orlando, J. J.; Piety, C. A.; Nicovich, J. M.; McKee, M. L.; Wine, P. H. *J. Phys. Chem. A* **2005**, *109*, 6659.

(83) Wine, P. H.; Nicovich, J. M.; McKee, M. L.; Kleissas, K. M.; Parthasarathy, S.; Pope, F. D.; Pegus, A. T. *Intl. Symp. Gas Kinet., 18th* **2004**.

(84) Arsene, C.; Barnes, I.; Albu, M. *Intl. Symp. Gas Kinet., 17th* **2002**.

(85) See for example, Atkinson, R.; Baulch, D. L.; Cox, R. A.; Hampson, R. F. Jr.; Kerr, J. A.; Rossi, M. J.; Troe, J. *J. Phys. Chem. Ref. Data* **1999**, *28*, 191.

(86) Arsene, C.; Barnes, I.; Becker, K. H.; Schneider, W. F.; Wallington, T. T.; Mihalopoulos, N.; Patroescu-Klotz, I. V. *Environ. Sci. Technol.* **2002,** *36*, 5155.

(87) Ballesteros, B.; Jensen, N. R.; Hjorth, J. *J. Atmos. Chem.* **2002**, *43*, 135.

(88) McKee, M. L.; Wine, P. H. Manuscript in preparation for submission to *Chem. Rev.*

(89) Prinn, R. G.; Huang, J.; Weiss, R. F.; Cunnold, D. M.; Fraser, P. J.; Simmonds, P. G.; McCulloch, A.; Harth, C.; Salameh, P.; O′Doherty, S.; Wang, R. H. J.; Porter, L.; Miller, B. R. *Science* **2001**, *292*, 1882.

(90) See, for example: Jefferson, A.; Tanner, D. J.; Eisele, F. L.; Davis, D. D.; Chen, G.; Crawford, J.; Huey, J. W.; Torres, A. L.; Berresheim, H. *J. Geophys. Res.-Atmos.* **1998**, *103*, 1647.

(91) Wingenter, O. W.; Sive, B. C.; Blake, N. J.; Blake, D. R.; Rowland, F. S. *J. Geophys. Res.-Atmos.* **2005**, *110*, D20308, doi: 10.1029/2005JD005875.

(92) Young, D. C.; McKee, M. L. *Bonding in Gas-Phase Sulfur Radicals*; Computational Chemistry: Reviews of Current Trends Volume 4; Leszczynski, J., Ed.; World Scientific: Singapore, 1999; pp 149−178.

(93) Thompson, K. C.; Canosa-Mas, C. E.; Wayne, R. P. *Phys. Chem. Chem. Phys.* **2002**, *4*, 4133.

(94) Resende, S. M.; De Almeida, W. B. *J. Phys. Chem. A* **1997**, *101*, 9738.

(95) Curtiss, L. A.; Redfern, P. C.; Raghavachari, K.; Rassolov, V.; Pople, J. A. *J. Chem. Phys.* **1999**, *110*, 4703.

(96) Enami, S.; Nakano, N.; Hashimoto, S.; Kawasaki, M.; Aloisio, S.; Francisco, J. S. *J. Phys. Chem. A* **2004**, *108*, 7785.

(97) McKee, M. L. *J. Phys. Chem. A* **2003**, *107*, 6819. Erratum. **2003**, *107*, 10221.

(98) Uchimaru, T.; Tsuzuki, S.; Sugie, M.; Tokuhashi, K.; Sekiya, A. *Chem. Phys. Lett.* **2005**, *408*, 216.

(99) González-García, N.; González-Lafont, A.; Lluch, J. M. *J. Comput. Chem.* **2005**, *26*, 569.

(100) Diaz-de-Mera, Y.; Aranda, A.; Rodriguez, D.; Lopez, R.; Cabanas, B.; Martinez, E. *J. Phys. Chem. A* **2002**, *106*, 8627.

(101) Wine, P. H.; Nicovich, J. M.; Stickel, R. E.; Zhao, Z.; Shackelford, C. J.; Kreutter, K. D.; Daykin, E. P.; Wang, S. In *The Tropospheric Chemistry of Ozone in the Polar Regions*; Niki, H., Becker, K. H., Eds.; NATO ASI Series, Volume I7; Springer-Verlag: Berlin, 1993; pp 385−395.

(102) Nakano, Y.; Goto, M.; Hashimoto, S.; Kawasaki, M.; Wallington, T. J. *J. Phys. Chem. A* **2001**, *105*, 11045.

(103) Wine, P. H.; Kreutter, N. M.; Gump, C. A.; Ravishankara, A. R. *J. Phys. Chem.* **1981**, *85*, 2660.

(104) Hynes, A. J.; Semmes, D. H.; Wine, P. H. *J. Phys. Chem.* **1986**, *90*, 4148.

(105) Hsu, Y.-C.; Chen, D.-S.; Lee, Y.-P. *Int. J. Chem. Kinet.* **1987**, *19*, 1073.

(106) Abbatt, J. P. D.; Fentner, F. F.; Anderson, J. G. *J. Phys. Chem.* **1992**, *96*, 1780.

(107) Barone, S. B.; Turnipseed, A. A.; Ravishankara, A. R. *J. Phys. Chem.* **1996**, *100*, 14694.

(108) Hynes, A. J.; Stoker, R. B.; Pounds, A. J.; McKay, T.; Bradshaw, J. D.; Nicovich, J. M.; Wine, P. H. *J. Phys. Chem.* **1995**, *99*, 16967.

(109) Williams, M. B.; Campuzano-Jost, P.; Bauer, D.; Hynes, A. J. *Chem. Phys. Lett.* **2001**, *344*, 61.

(110) Wang, Y.; Liu, S. C.; Wine, P. H.; Davis, D. D.; Sandholm, S. T.; Atlas, E. L.; Avery, M. A.; Blake, D. R.; Blake, N. J.; Brune, W. H.; Heikes, B. G.; Sachse, G. W.; Shetter, R. E.; Singh, H. B.; Talbot, R. W.; Tan, D. *J. Geophys. Res.* **2001**, *106*, 32733.